IJE TRANSACTIONS A: Basics Vol. 31, No. 10, (October 2018) 1773-1781

International Journal of Engineering

Journal Homepage: www.ije.ir

Probability Approach for Prediction of Pitting Corrosion Fatigue Life of Custom 450 Steel

A. Salarvand[a], E. Poursaiedi*[b], A. Azizpour[b]

[a] *Department of Mechanical Engineering, Islamic Azad University, Doroud Branch, Iran*
[b] *Department of Mechanical Engineering ,University of Zanjan, Zanjan, Iran*

P A P E R I N F O

Paper history:
Received 10 November 2017
Received in revised form 09 June 2018
Accepted 17 August 2018

Keywords:
Corrosion Fatigue
Corrosion Pit
Crack Propagation
High Cycle Fatigue
Custom 450 Steel

A B S T R A C T

In this study, the pitting type of corrosion growth characteristics, fatigue crack initiation and propagation behavior; axial fatigue tests were carried out on precipitation hardened martensitic Custom 450 steel in the air and 3.5wt% NaCl solution. Using the ratio of the depth to the half-width of the pits; (a/c)= 1.5±0.2 the corrosion pit depth growth law was obtained as a function of stress amplitude and elapsed time, t. Fatigue crack growth rates were determined in the near threshold stress intensity factors regime (Δk_{th}). A model was presented for estimation of corrosion fatigue life based on the time to reach critical pit depth (as crack initiation) and crack propagation life. Then. S-N curves were obtained both in air and NaCl solution from axial fatigue testing. Comparison of data from the proposed model and the experimental results (S-N curves) showed good agreement.

***doi**: 10.5829/ije.2018.31.10a.21*

1. INTRODUCTION

Gas turbine compressor sections move large volumes of air that often contain significant amounts of airborne salt, water, and potentially corrosive gaseous species that can combine to form destructive acidic compounds. Precipitation-hardened martensitic Custom 450 stainless steel is used to make gas turbine compressor blades because it offers high strength, toughness and good corrosion resistance. Premature fracture failure in the first row of rotating blades of gas turbine compressors installed at a seaside power plant has been observed. Previous studies [1-3] revealed that the failure was caused by crack propagation from initial surface pitting that formed under a high cycle fatigue mechanism. The corrosion pits act as pre-existing flaws in the material to nucleate fatigue cracks.

Linear elastic fracture mechanics have been used in several investigations on durable cyclic loading in the presence of pitting corrosion [4-7]. The results of these models depend on the material and test conditions. Creating a relationship between pit size and elapsed time in pit development has attracted a number of studies. Sriraman et al. [8] developed a model that considered the coexistence of a corrosive environment and fatigue loading conditions and took into account the influence of cyclic stress in pitting corrosion. Optical profilometry and Weibull functions to characterize pit depth and diameter distributions were used by Cavanaugh and that found pit growth kinetics varied by the environment, but most followed approximately $t^{1/3}$ kinetics [9]. Sriraman proposed pit depth a_p as proportional to the cube root of t through the relationship $a_p=Bt^{1/3}$ [10].

Ishihara et al. [11] investigated corrosion pit growth characteristics and fatigue crack initiation and propagation behavior of the aluminum alloy 2024-T3 in 3% NaCl solution in detail. They developed a corrosion pit growth law as a function of stress amplitude σ_a and an elapsed time *t.* Shi and Mahadevan [12] studied the damage tolerance approach for probabilistic pitting corrosion fatigue life prediction and found that pit nucleation time and the material constant for short crack growth (Δk_{th}) are the two most important random variables affecting corrosion fatigue life. Bastidas-Arteaga [13] developed a model to predict corrosion fatigue lifetime. The results showed that the coupled

*Corresponding author E-mail: *epsaeidi@gmail.com* (E. Poursaeidi)

Please cite this article as: A. Salarvand, E. Poursaiedi, A. Azizpour, Probability Approach for Prediction of Pitting Corrosion Fatigue Life of Custom 450 Steel, International Journal of Engineering (IJE), IJE TRANSACTIONS A: Basics Vol. 31, No. 10, (October 2018) 1773-1781

effect of corrosion and fatigue on a structure strongly affects performance and can significantly decrease the expected lifetime.

Lin and Tsai [14] evaluated corrosion fatigue behavior of a 15Cr–6Ni Custom 450 steel under three different aging conditions to characterize the effects of aging treatment on corrosion fatigue (CF) resistance in laboratory air and 3.5 wt% NaCl solutions. Fatigue resistance in all three tempers decreased dramatically in the aqueous NaCl environment according to S–N results. In addition, it was found that the peak-aged steel temper exhibited highest CF resistance while, the over-aged sample had the lowest value. Some authors [15, 16] have dealt with fatigue life estimation of pitted 12% Cr steel using the short crack approach [17] to estimate the durable cyclic stress according to pit size.

Additional research [18-24] has been conducted on pitting corrosion fatigue in various materials, but none thus far have examined the growth of pits and transition from pit to crack in C450 steel. Following previous investigations by the authors, the present study focuses on the mechanism of growth of corrosion pits under the cyclic loading and prediction of corrosion fatigue life using the corrosion pit growth law for Custom 450 steel.

2. MATERIALS AND METHODS

2. 1. Materials Samples of Custom 450 steel were prepared by cutting and machining of scrap blades of a gas turbine compressor. The results of quantometery and chemical analysis of a sample of the materials are shown in Table 1. This type of steel was heated at 1030 °C for 0.5 h and then was quenched in water. Precipitation hardening was then carried out at 530 °C (1050 °F) for 4 h [25] to obtain a microhardness of 310±10 HV. The mechanical properties of the material are shown in Table 2.

TABLE 1. Chemical analysis of C450 stainless steel

Element	Wt (%)
C	0.027
Mn	0.6
Si	0.245
P	0.0166
Co	0.0604
Cr	15.17
Ni	6.43
Mo	0.79
Cu	1.48
Nb	0.35
Fe	Blance

TABLE 2. Mechanical properties of Custom 450 at room temperature (provided by the supplier)

Tensile strength (MPa)	Yield strength (MPa)	Elongation A (%)	Hardness (HV)
1100	1060	21	310

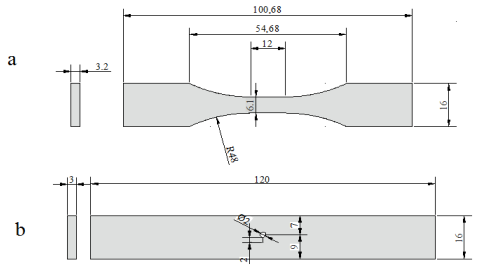

Figure 1. Specimens used to test: (a) fatigue (S-N) and; (b) FCGR. All dimensions are in mm

2. 2. Test Sample Preparation Twenty-five fatigue specimens were made according to ASTM E466 standards [26] for fatigue testing and measurement of corrosion pit dimensions (Figure 1(a)). Also six specimens were prepared to measure fatigue crack growth rate (FCGR) (Figure 1(b)). The sample surfaces were initially machined and then ground and polished using grade 400 to 4000 abrasive papers. The surfaces were fully polished and mirrored using cloth and fluids with abrasive nano-silica particles. Plate-shaped samples with a starter notch were used to measure FCGR and to determine the threshold stress intensity factor (Figure 1(b)). A hole 2 mm in diameter was drilled in the middle of the sample then a groove crack 0.35 mm wide and 2 mm length was created by electrical discharge machining on one side of the hole.

3. TESTING PROCEDURES

3. 1. Corrosion Pit Depth Measurement Under Cyclic Loading An axial fatigue testing machine was used to produce the Corrosion Fatigue (CF) pits. During the pitting and corrosion fatigue tests, samples were placed in a solution of 3.5% wt NaCl under cyclic loading in the form of a sine wave at a frequency of 20 Hz and stress ratio of R = 0.1 at stress amplitudes of 0, 150, 250, 300 and 325 MPa.

To evaluate the corrosion fatigue pitting, a corrosion cell consisting of a sealed chamber was designed. The corrosion cell covered part of the sample surface and the saline solution was pumped into the cell by a pump from a tank (Figure 2) and then returned to the main tank. Dissolved O_2 in the solution was kept at the saturation point by passing air through it. The solution temperature was about 25 °C. Repliset method was used to evaluate the corrosion pit geometry and measure the dimensions. In this method, the sample is pressed onto

the surface of the polymer material and the effects of pits and surface roughness of the sample remain on the surface of the polymer material in raised relief (Figure 3).

The surface topography of the samples was produced using Repliset method and CF tests were carried out on the samples. After specified periods of time, testing was halted and the sample surface features were again recorded and the test continued. The height of Repliset relief patterns represent the depth of the corrosion pits and were measured using the focused focal point method. The diameter of the relief on the surface of Repliset was measured and found to be equivalent to pit diameter. The time variations of the maximum pit depth distribution were then measured. A portion of the sample surface 14.4 mm^2 in the area (right image of Figure 4) was divided into 12 parts, each 1.2 mm^2 in area. In order to better observation of micro pits, 12 images were taken on each area (left image of Figure 4). The biggest pit was determined in each area and its dimensions measured.

3. 2. Fatigue Tests Axial tests based on ASTM E466 were carried out on a servo hydraulic fatigue test machine to determine the S-N curves at a constant sine stress amplitude at a frequency of 20 Hz with a stress ratio of R = 0.1 at room temperature. Measurement of FCGR began at a frequency of 20 Hz (55 Mpa< σ < 550 Mpa; R = 0.1) with a high crack growth rate of (10^{-8} – 10^{-9}) m/cycle. After crack advance was detected with the length of 1mm, Δk was gradually decreased and this process was repeated until crack growth arrested. The lowest value recorded for Δk was considered as Δk_{th}.

4. TEST RESULTS

4. 1. Corrosion Pits Formation During Corrosion Fatigue Figure 5 shows images of corrosion pit formation taken by an optical microscope under cyclic loading at a stress amplitude of σ_a = 250 MPa and stress ratio of R = 0.1. The figure shows pit formation of the sample surface before the test and after 3 and 6 h of testing. As seen, the size and number of the pits increased as the time increased.

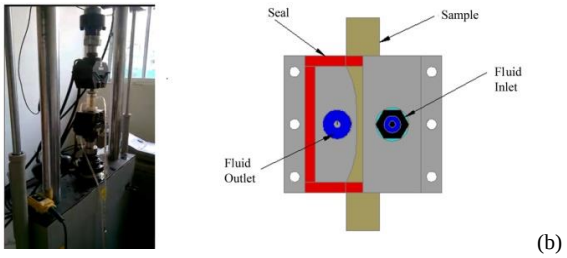

(a) (b)

Figure 2. Fatigue testing machine: (a) Running the corrosion fatigue test; (b) corrosion cell

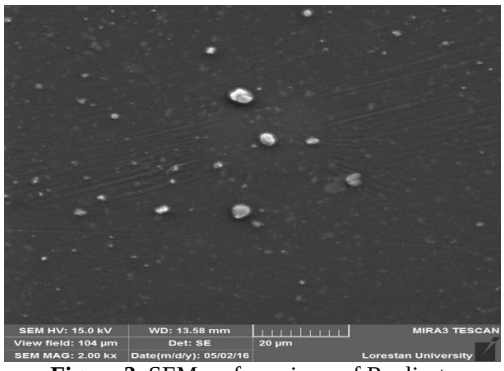

Figure 3. SEM surface views of Replisets

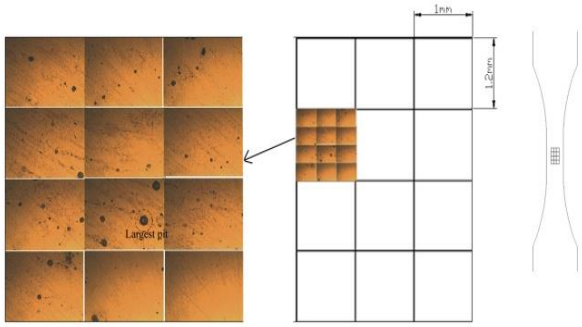

Figure 4. Surface view divided into 12 parts and 12 photographs of the parts

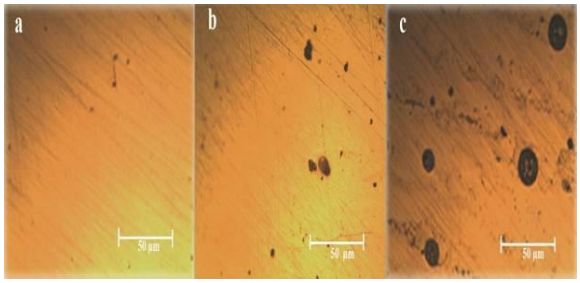

Figure 5. Successive images of corrosion pits during CF testing (σ_a = 250 MPa, R = 0.1, f = 20 Hz): (a) before testing (t = 0); (b) t = 3 h; (c) t = 6 h

4. 2. Time Versus Maximum Pit Depth Distribution Studies have shown that it is difficult to determine the exact behavior and growth of corrosion pits. The pits that have the same diameter and depth do not necessarily grow in a similar fashion. One reason for this is that measurement of pit dimensions is influenced by individual characteristics such as choice of the pit and by observations made. For this reason, the variations in pit formation over time was investigated as maximum pit depth distribution.

A portion of the surface of a sample was divided into 12 parts of 1.2 mm^2 in size (Figure 4). The maximum pit depth was measured for each part using Repliset method (see section 3.1). An extreme-value

distribution was plotted to obtain the maximum pit depth distribution. Figure 6 shows time versus the maximum pit depth distribution plotted on the largest extreme-value. The data was plotted at stress amplitudes of 0, 150, 250, 300 and 325 MPa. As the figure shows, the distribution of the maximum pit depth moved to the right as time increased, indicating pit depth increased as time increased. It was also observed that the maximum pit depth distribution was linear, which means that the distribution of the maximum pit depth (a_i) can be expressed as a double exponential relationship as follows:

$$F_{a_i} = Exp\{-Exp\left[\frac{-(a_i-\alpha)}{\mu}\right]\} \quad (1)$$

where μ denotes scale and α denotes location parameter.

4. 3. Effect of Stress Amplitude on the Time Variation of the Distribution of the Maximum Pit Depth Figure 7 shows the distribution of the maximum pit depth, $F(a_i)$, for amplitudes of 150, 250, 300 and 325 MPa with constant elapsed time to clarify the effect of stress amplitude on the time variation of the distribution, $F(ai)$. As seen, the growth rate of the pits increased as the stress amplitude increased. The effect of stress amplitude on the growth rate of pit depth is apparent. To investigate the effect of elapsed time on the maximum pit depth distribution, location parameter (α) in Equation (1) from Figure 8 was used. By plotting the log-log curve for α versus time (t) for different stress amplitudes, variations in α according to stress amplitude can be determined (Figure 8).

4. 4. Corrosion Pit Growth Formulation The test results show that the growth rate of corrosion pit depth is affected by cyclic stress amplitude. Results of the previous research have shown that the effect of loading frequency on corrosion pit growth is insignificant [11]. So far, Equation (2) was used as a corrosion pit growth law [7]:

$$a = At^{\beta} \quad (2)$$

where a is corrosion pit depth, t is the elapsed time and A and β are constants determined by testing. Because stress amplitude σ_a effects on corrosion pit growth, it should be considered in the equation in addition to elapsed time (t). Equation (2) has been modified to include stress amplitude as:

$$a = A(\sigma_a)t^{\beta} \quad (3)$$

where $A(\sigma_a)$ is the stress amplitude function and β is the power index of time. Location parameter α for maximum pit depth distribution was used instead of corrosion pit depth (a), because this parameter represents the highst density of data which can be extracted for maximum pit depth estimation in extreme-value theory. The values for $A(\sigma_a)$ and β in Equation (3) were obtained by calculating the gradient and intercept of the lines in Figure 8 and are shown in Table 3.

By averaging the values for β for different stress amplitudes, a value of 0.34 was determined. Using a log-normal plot of the $A(\sigma_a)$ values versus σ_a and measuring the resulting gradient and intercept (Figure 9) produces Equation (4) for $A(\sigma_a)$. Corrosion pit growth law is expressed in Equation (5):

$$A(\sigma_a) = 3.826(1.0045)^{\sigma_a} \quad (4)$$

$$a \cong \alpha = 3.826(1.0045)^{\sigma_a} t^{0.34} \quad (5)$$

where a (μm), σ_a (MPa) and t (h) are pit depth, cyclic stress amplitude and elapsed time, respectively.m

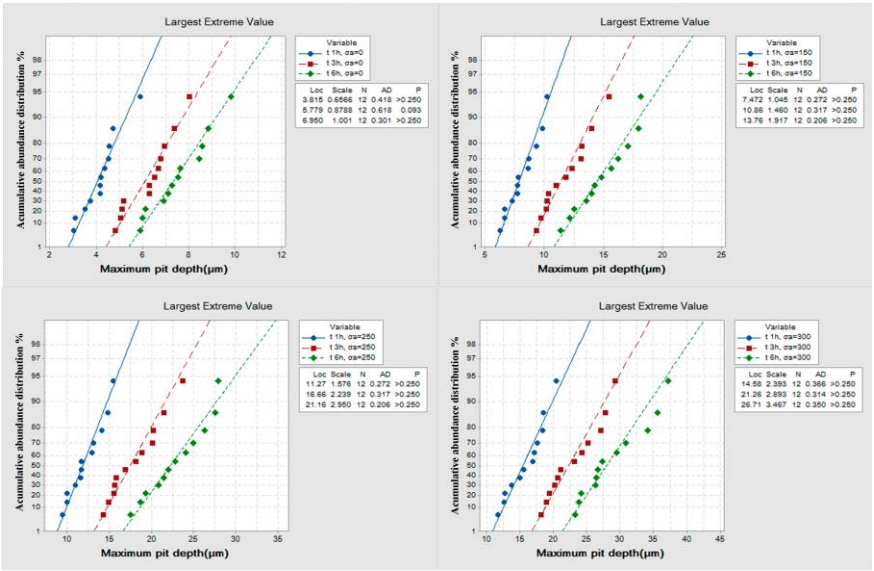

Figure 6. Time versus maximum pit depth distribution plotted as extreme-value distribution

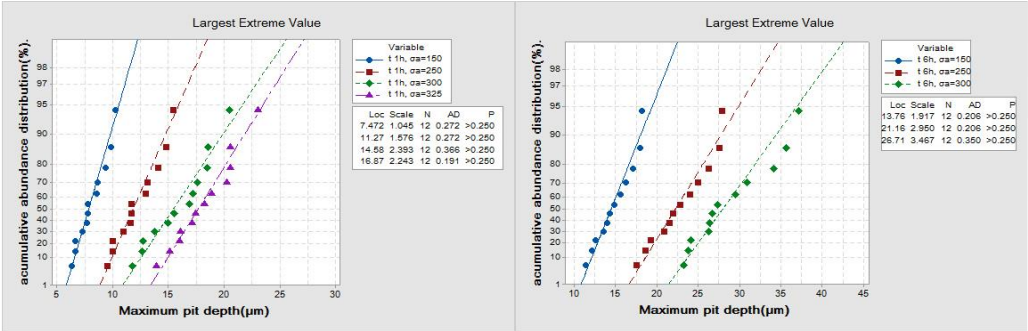

Figure 7. Maximum pit depth distribution ($F(a_i)$) for amplitudes of 150, 250, 300 and 325MPa at t = 1 h and t = 6 h

4. 5. Geometric Characteristics of Pits Scanning electron microscopy (SEM) and optical microscopy of the specimen surfaces under CF showed that most pits were irregular in shape and that pits had different geometries; however, they can be assumed to be roughly semi-elliptical (Figure 10). Measurement of pit dimensions showed that the ratio of the depth to the half-width of the pits can be expressed as: a/c = 1.5 ± 0.2. Cross-sections of pits that were initially circular were shown to become elliptical gradually under the applied stress, particularly when the stress concentration occurred on both sides.

4. 6. Crack Initiation Criteria It has been proven that cracks initiate from corrosion pits which arise during CF [20, 21]. To determine the status of crack initiation from a corrosion pit, CF tests were conducted using axial loading on the flat samples. The assumption that pits at the threshold of cracking will behave like cracks is not uncommon. Several relationships have been suggested to calculate the threshold stress intensity factor based on pit dimension using linear elastic fracture mechanics (LEFM). One example is:

$$\Delta K_{th} = \gamma . \Delta\sigma_{th} \sqrt{\pi a} \quad (6)$$

where ΔK_{th} is the threshold stress intensity factor range, $\Delta\sigma_{th}$ is the threshold fatigue strength range, a is the depth of the pit and γ is a geometrical factor equal to 0.67 for semicircle surface cracks [5, 22].

Murakami [23] used Equation (7) to calculate the critical stress intensity factor for crack initiation when pits become crack ($\Delta K_{pit \rightarrow areak}$) of irregular surface cracks as:

$$\Delta K_{p \rightarrow c} = 0.65 \Delta\sigma \sqrt{\pi \sqrt{area_{p \rightarrow c}}} \quad (7)$$

where $\Delta\sigma$ is the range of applied tensile stress and $area_{p \rightarrow c}$ is the pit cross-section in the direction perpendicular to the applied tensile load. Assuming that the value of $\Delta K_{p \rightarrow c} = \Delta K_{th}$, $area_{p \rightarrow c}$ can be calculated for different stress amplitudes. The value of ΔK_{th} can be obtained from the FCGR curve. Assuming that critical pit depth a_{th} equals $\sqrt{area_{p \rightarrow c}}$, Equation (5) can be used to calculate the time required to reach critical pit depth and crack initiation for each stress amplitude.

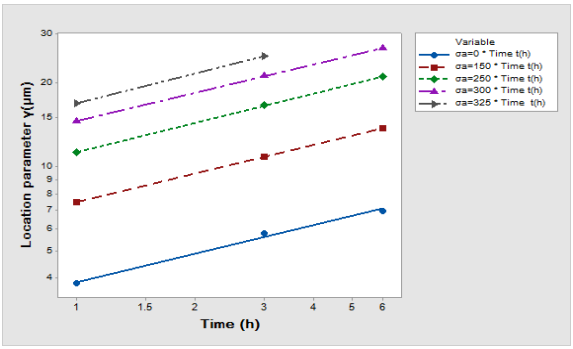

Figure 8. Effect of stress amplitudes on the relationship between location parameter α and an elapsed time, t

TABLE 3. Values of $A(\sigma_a)$ and β for each stress amplitude

Stress Amplitude (σ_a) (MPa)	A(σ_a)	β
0	3.861	0.338
150	7.471	0.340
250	11.272	0.352
300	14.588	0.338
325	16.865	0.356

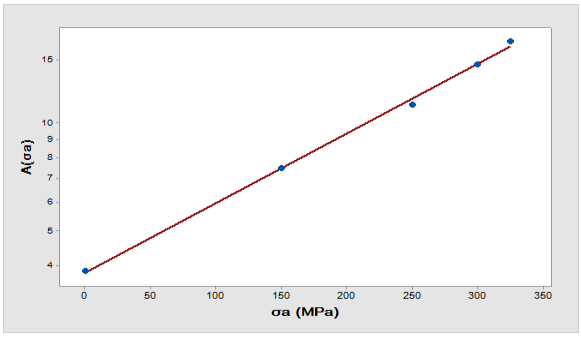

Figure 9. Variation in $A(\sigma_a)$ as a function of stress amplitude

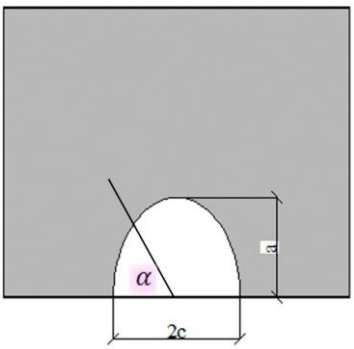

Figure 10. General schematic fracture surface including a pit

4. 7. Determination of FCGR Curves in Air and Saline Solution FCGR measurement was carried out in the near-threshold regime at a stress ratio of R = 0.1. Testing was done in both air and a solution of 3.5% wt NaCl. Figure 11 shows the two FCGR curves. The threshold stress intensity factor range (ΔK_{th}), where the crack growth rate is less than $1E^{-10}\frac{m}{cycle}$, for the saline environment and air were 3.3 and 3.8 MPa $\sqrt{m}$, respectively. As seen from the figure, the general relationship according to the Paris equation takes the form:

$$\frac{da}{dN} = C(\Delta K)^m \tag{8}$$

where a and ΔK are the depth of the crack and the stress intensity factor range, respectively, and C and m are material constants.

Assuming that the shape of the pit is semi-ellipsoidal, Equation (9) can be used to calculate the stress intensity factor [24] as:

$$\varphi = \frac{3\pi}{8} + \frac{\pi}{8}\left(\frac{a}{c}\right)^2,$$
$$K_I = \frac{1/12\sigma\sqrt{\pi a}}{\varphi}\left(\sin^2\alpha + \left(\frac{a}{c}\right)^2\cos^2\alpha\right)^{1/4} \tag{9}$$

Assuming that c/a = 0.667, the stress intensity factor becomes:

$$\Delta K = 0.66\Delta\sigma\sqrt{\pi a} \tag{10}$$

4. 8. S-N Tests Axial fatigue test data and S-N curves in the air and saline solution are shown in Figure 12 at a frequency of 20 Hz and a stress ratio of R = 0.1 for smooth and polished samples.The tests continued to failure the samples. The results show that the material fatigue strength decreased in the corrosive environments. The maximum stress applied to the sample at 555 to 930 MPa (0.5 to 0.85 σ_u) changed according to the sample and environmental condition. The solid lines in Figure 12 denote the testing data for which the following parametric relation can be considered:

$$S = \sigma_f' N_f^n \tag{11}$$

where S is the maximum alternative stress, N_f is the number of failure cycles, σ_f' is the fatigue strength coefficient, and n is the fatigue exponent. Table 4 summarizes the values of σ_f' and n.

5. DISCUSSION

5. 1. Estimation of Crack Initiation Life Using relation $N = ft$ between the number of stress cycles N and time t which f is the cyclic stress frequency and combining it with Equation (5) produces crack initiation life (N_i) as:

$$N_i = 3600 f * \sqrt[\beta]{\frac{a_{th}}{3.826(1.0045)^{\sigma_a}}} \tag{12}$$

Substituting $\Delta K_{p\to c} = 3.3\ MPa\sqrt{m}$ obtained from the FCGR curve for the 3.5% wtNaCl solution environment and $area_{p\to c} = \frac{\pi a_{th} c_{th}}{2}$ and assuming $\frac{c_{th}}{a_{th}} = 0.667$ results in:

$$\sqrt{area_{p\to c}} \cong a_{th} \tag{13}$$

Substituting Equation (13) into Equation (7) produces:

$$a_{th} = \left(\frac{\Delta k_{th}}{0.65\Delta\sigma\sqrt{\pi}}\right)^2 \tag{14}$$

Now a_{th} can be obtained for any range of stress $\Delta\sigma$ from Equation (14) and, by substituting it into Equation(12), crack initiation life N_i can be calculated as the critical pit life.

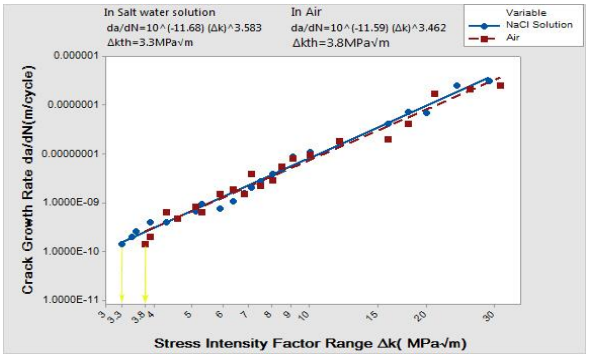

Figure 11. FCGR curves for cracks emanating from pits in the air and 3.5% NaCl solution

TABLE 4. Parameters used in Equation (11)

Material & test environment	σ_f' (MPa)	n
C450- in air	2142.9	-0.0798
C450-in salt solution	2666.8	-0.1078

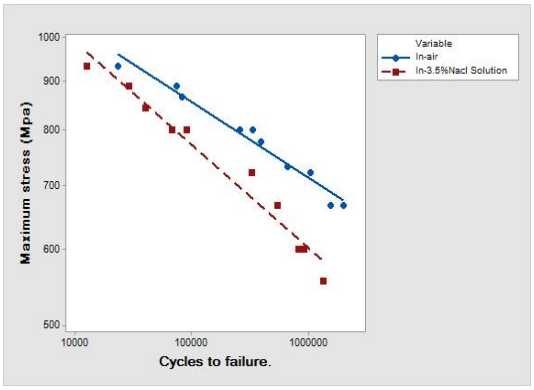

Figure 12. S-N curves in air and 3.5 wt% NaCl solution

5. 2. Estimation of Crack Growth Life With substituting Equation (10) in to the Equation (8) and integration from a_{th} (critical pit depth) to $a_f = \frac{w}{2} = 0.003m$ (w width of the sample), crack propagation life N_p becomes:

$$N_p = \frac{-2\pi^{\frac{-m}{2}}(1.23\Delta\sigma)^{-m}}{C(m-2)}\left[a_f^{\frac{2-m}{2}} - a_{th}^{\frac{2-m}{2}}\right] \quad (15)$$

Corrosion fatigue life N_f is estimated to be the sum of crack initiation life N_i and crack propagation life N_p.

5. 3. Validation of Corrosion Fatigue Model In order to evaluate the accuracy of the prediction for results of the presented model, fractographic images of the fracture surface of a number of specimens (that failed during CF testing used to determine the S-N curves) were analyzed by SEM. Figure 13 shows fracture surface of a test sample in a solution of 3.5% wt NaCl for which σ_{max} = 667 MPa and R = 0.1 at 20 Hz frequency that failed after 472,351 cycles. The source of crack initiation is determined by the convergence of the fracture marking lines. As the figure indicates, the critical pit cross-section is $area_{p\to c} = 600\ \mu m^2$ and a_{th} = 24 µm.

In the proposed model, by assuming $\Delta K_{p\to c} = 3.3\ MPa\sqrt{m}$ from the FCGR curve for this material, the critical cross-section of the pit for stress range $\Delta\sigma$ = 600 MPa equals $area_{p\to c} = 519\ \mu m^2$, $a_{th} = 22.8\mu_m$ and, thus, $N_i = 265703$, $N_p = 164090$ and $N_f = 429793$ cycles. This represents about a %10 deviation from the test results (472,351 cycles).

Figure 14 compares the tests results and the estimated corrosion fatigue life from the proposed model. As seen, the estimated results are in good agreement with the experimental data, although estimations show a shorter life span than the experimental results. This may have resulted from the absence of consideration of the onset time (before the formation of the pit) of the initial pit.

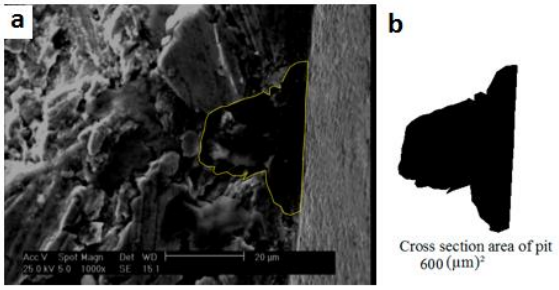

Figure 13. The fracture surface of the test sample in 3.5%wt NaCl solution and the cross-section area of the pit

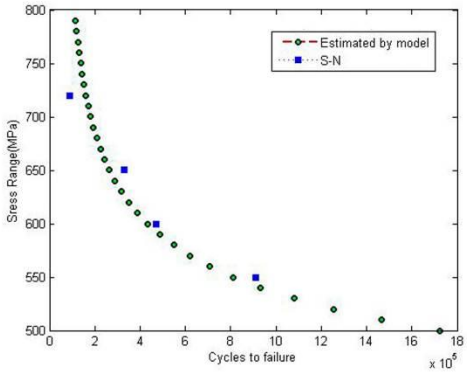

Figure 14. Comparison of estimated and experimental corrosion fatigue life

With a decrease in stress amplitude, the corrosion pit growth rate decreased, the time span of crack initiation increased and CF life also increased. At low stress amplitudes, most CF life relates to the growth of the corrosion pit. This is why a complete understanding of the growth mechanisms of a corrosion pit is important for fatigue life assessment.

6. CONCLUSION

The present study investigated pitting corrosion fatigue behavior of precipitation hardened Custom 450 steel using tensile axial fatigue testing at a 3.5% wt NaCl solution. Fatigue crack growth characteristics and the behavior of fatigue pit initiation and its propagation were evaluated. Measurement of the fatigue crack growth rate (FCGR) near the threshold regime and S-N tests in the high cycle regime was conducted on perfectly smooth samples in air and 3.5%wt NaCl solution. The results are summarized below.

1. Corrosion pit depth (µm) can be presented as a function of stress amplitude (MPa) and elapsed time (h) as $a = 3.826(1.0045)^{\sigma_a} t^{0.34}$.
2. The FCGR curves showed that the stress intensity factor threshold ΔK_{th} value in a saline solution was less than in air (3.3 and 3.8 MPa $\sqrt{m}$, respectively). These values can be used as the

critical stress intensity factor for crack initiation $\Delta k_{p\to c}$ from the corrosion pit.

3. Crack propagation life in saline solution was calculated using the relationship $\frac{da}{dN} = 10^{-1168}(\Delta K)^{3.583}$ from the FCGR curve. Corrosion fatigue life N_f can be calculated as the sum of crack initiation life (N_i; calculated using the law of corrosion pit growth under critical conditions) and crack propagation life (N_p).

4. Results of the proposed model and the relationships used to determine the corrosion fatigue life were in good agreement with the experimental results on the S-N curve.

5. The S-N curves showed that the fatigue limit in the saline solution was less than in air and this difference was more evident at lower stress amplitudes. At the low stress amplitudes, the corrosion pit growth was primarily related to fatigue life.

7. REFRENCES

1. Poursaeidi, E., Sanaieei, M., and Bakhtyari, H., "Life Estimate of a Compressor Blade through Fractography", ***International Journal of Engineering - Transactions A: Basics***, Vol. 26, No. 4, (2012), 393–400.
2. Poursaeidi, E., Babaei, A., Behrouzshad, F., and Mohammadi Arhani, M.R., "Failure analysis of an axial compressor first row rotating blades", ***Engineering Failure Analysis***, Vol. 28, (2013), 25–33.
3. Poursaeidi, E., and Pedram, O., "An Outrun Competition of Corrosion Fatigue and Stress Corrosion Cracking on Crack Initiation in a Compressor Blade", ***International Journal of Engineering - Transactions B: Applications***, Vol. 27, No. 5, (2013), 785–792.
4. Lindley, T.C., Mcintyre, P., and Trant, P.J., "Fatigue-crack initiation at corrosion pits", ***Metals Technology***, Vol. 9, No. 1, (1982), 135–142.
5. Kondo, Y., "Prediction of fatigue crack initation life based on pit growth", ***Corrosion***, Vol. 45, No. 1, (1989), 7–11.
6. Kawai, S., and Kasai, K., "Considerations of Allowable Stress of Corrosion Fatigue (Focussed on the Influence of Pitting)", ***Fatigue & Fracture of Engineering Materials & Structures***, Vol. 8, No. 2, (1985), 115–127.
7. Turnbull, A., McCartney, L.N., and Zhou, S., "A model to predict the evolution of pitting corrosion and the pit-to-crack transition incorporating statistically distributed input parameters", ***Corrosion Science***, Vol. 48, No. 8, (2006), 2084–2105.
8. Sriraman, M.R., and Pidaparti, R.M., "Crack Initiation Life of Materials Under Combined Pitting Corrosion and Cyclic Loading", ***Journal of Materials Engineering and Performance***, Vol. 19, No. 1, (2010), 7–12.
9. Cavanaugh, M., Buchheit, R., and Birbilis, N., "Modeling the environmental dependence of pit growth using neural network approaches", ***Corrosion Science***, Vol. 52, No. 9, (2010), 3070–3077.
10. Sriraman, M.R., and Pidaparti, R.M., "Life Prediction of Aircraft Aluminum Subjected to Pitting Corrosion Under Fatigue Conditions", ***Journal of Aircraft***, Vol. 46, No. 4, (2009), 1253–1259.
11. Ishihara, S., Saka, S., Nan, Z.Y., Goshima, T., and Sunada, S., "Prediction of Corrosion Fatigue Lives of Aluminium Alloy on The Basis of Corrosion Pit Growth Law", ***Fatigue and Fracture of Engineering Materials and Structures***, Vol. 29, No. 6, (2006), 472–480.
12. Shi Pan, M.S., "Damage tolerance approach for probabilistic pitting corrosion fatigue life prediction", ***Engineering Fracture Mechanics***, Vol. 68, No. 13, (2001), 1493–1507.
13. Bastidas-Arteaga, E., Bressolette, P., Chateauneuf, A., and Sánchez-Silva, M., "Probabilistic lifetime assessment of RC structures under coupled corrosion–fatigue deterioration processes", ***Structural Safety***, Vol. 31, No. 1, (2009), 84–96.
14. Lin, C.K., and Tsai, W.J., "Corrosion fatigue behaviour of a 15Cr-6Ni precipitation-hardening stainless steel in different tempers", ***Fatigue and Fracture of Engineering Materials and Structures***, Vol. 23, No. 6, (2000), 489–497.
15. Schonbauer, B.M., Stanzl-Tschegg, S.E., Perlega, A., Salzman, R.N., Rieger, N.F., Zhou, S., Turnbull, A., and Gandy, D., "Fatigue life estimation of pitted 12% Cr steam turbine blade steel in different environments and at different stress ratios", ***International Journal of Fatigue***, Vol. 65, (2014), 33–43.
16. Schonbauer, B.M., Perlega, A., Karr, U.P., Gandy, D., and Stanzl-Tschegg, S.E., "Pit-to-crack transition under cyclic loading in 12% Cr steam turbine blade steel", ***International Journal of Fatigue***, Vol. 76, (2015), 19–32.
17. El Haddad, M.H., Topper, T.H., and Smith, K.N., "Prediction of non propagating cracks", ***Engineering Fracture Mechanics***, Vol. 11, No. 3, (1979), 575–584.
18. Lindström, R., Johansson, L., Thompson, G., Skeldon, P., and Svensson, J.E., "Corrosion of magnesium in humid air", ***Corrosion Science***, Vol. 46, No. 5, (2004), 1141-1158.
19. Harlow, D.G., and Wei, R.P., "A probability model for the growth of corrosion pits in aluminum alloys induced by constituent particles", ***Engineering Fracture Mechanics***, Vol. 59, No. 3, (1998), 305–325.
20. Medved, J.J., Breton, M., and Irving, P.E., "Corrosion pit size distributions and fatigue lives—a study of the EIFS technique for fatigue design in the presence of corrosion", ***International Journal of Fatigue***, Vol. 26, No. 1, (2004), 71–80.
21. Xie J., Alpas A.T., Northwood D.O., "A mechanism for the crack initiation of corrosion fatigue of Type 316L stainless steel in Hank's solution", ***Materials Characterization***, Vol. 48, No. 4, (2002), 271–277.
22. Ishihara, S., McEvily, A.J., and Shiozawa, K., "A fatigue-crack-growth-based analysis of two-step corrosion fatigue tests", ***Fatigue and Fracture of Engineering Materials and Structures***, Vol. 18, No. 11, (1995), 1311–1321.
23. Murakami, Y., "Metal Fatigue: Effects of Small Defects and Nonmetallic Inclusions", Elsevier, (2002).
24. Hayashi, K., and Abe, H., "Stress intensity factors for a semi-elliptical crack in the surface of a semi-infinite solid", ***International Journal of Fracture***, Vol. 16, No. 3, (1980), 275–285.
25. Kosa, T., and DeBold, T., "Effect of Heat Treatment and Microstructure on the Mechanical and Corrosion Properties of a Precipitation Hardenable Stainless Steel", In MiCon 78: Optimization of Processing, Properties, and Service Performance Through Microstructural Control, ASTM International, (1979), 367–392.
26. ASTM, "Standard Practice for Conducting Force Controlled Constant Amplitude Axial Fatigue Tests of Metallic Materials", ASTM E466 - 15, ASTM International, (2002), 4–8.

Probability Approach for Prediction of Pitting Corrosion Fatigue Life of Custom 450 Steel

A. Salarvand[a], E. Poursaiedi[b], A. Azizpour[b]

[a] *Department of Mechanical Engineering, Islamic Azad University, Doroud Branch, Iran*
[b] *Department of Mechanical Engineering ,University of Zanjan, Zanjan, Iran*

P A P E R I N F O

Paper history:
Received 10 November 2017
Received in revised form 09 june 2018
Accepted 17 August 2018

Keywords:
Corrosion Fatigue
Corrosion Pit
Crack Propagation
High Cycle Fatigue
Custom 450 Steel

چکیده

در این مطالعه، جهت ارزیابی مشخصات رشد حفره خوردگی، شروع ترک خستگی و رفتار رشد، آزمون‌های خستگی محوری بر روی فولاد مارتنزیتی رسوب سختی شده Custom 450 در هوا و محلول 3/5 درصد NaCl انجام شد. با در نظر گرفتن نسبت عمق به نصف عرض حفره‌ها بصورت $(\frac{a}{c}) = 1.5 \pm 0.2$، قانون رشد عمق حفره خوردگی به عنوان تابعی از دامنه تنش σ_a و زمان سپری شده t تخمین زده شد. نرخ‌های رشد ترک خستگی در نواحی نزدیک فاکتور شدت تنش آستانه تعیین شدند و مدلی برای تخمین عمر خستگی خوردگی بر اساس زمان رسیدن به عمق بحرانی حفره و عمر رشد ترک ارائه شد. سپس منحنی‌های S-N از آزمایش‌های خستگی محوری در هوا و محلول NaCl بدست آمدند که مقایسه داده‌های مدل پیشنهادی با نتایج آزمایشگاهی (منحنی‌های S-N) توافق خوبی را نشان داد.

***doi**: 10.5829/ije.2018.31.10a.21*